Journal of Structural Geology, Vol. 13, No. 8, pp. 955 to 966, 1991
Printed in Great Britain

0191-8141/91 $03.00+0.00

The influence of quartz textures on the seismic anisotropy in lower crustal granulites

GÜNTER BRAUN

Mineralogisch-Petrographisches Institut der Universität Kiel, 2300 Kiel, Germany

SIEGFRIED SIEGESMUND

Institut für Geologie und Dynamik der Lithosphäre, 3400 Göttingen, Germany

and

MICHAEL DAHMS

GKSS Forschungszentrum Geesthacht GmbH, 2054 Geesthacht, Germany

(*Received* 8 *February* 1990; *accepted in revised form* 25 *February* 1991)

Abstract—Analyses that are based on the spherical harmonic representation of the *orientation distribution function* (ODF) which can describe the three-dimensional nature of textures, can be used to evaluate the effective elastic response of quartz in polycrystalline aggregates and to account for the dependence of crystal and sample symmetries. The aggregate elastic constants are determined using the Voigt method by averaging overall orientations weighted by the ODF. The application of the results is given for three different, commonly observed, quartz textures. The directional dependence of the seismic wave velocities (V_p and shear wave splitting) that are calculated by ODF using the texture pole figures can also be shown using the respective single crystal velocities. The experimental seismic data at 400 MPa for a muscovite-bearing quartzite where most of the cracks are closed are in good agreement with the calculated velocity anisotropies (Voigt average) that are based on volume percentages of major minerals, the stiffness tensors of rock-forming minerals and the measured crystallographic orientation. The combination of the calculated elastic constants from different quartz textures together with plagioclase, muscovite, orthoclase, garnet and sillimanite explain the texture-related directional dependence of V_p, V_s and V_{ss} in lower crustal granulites. The results suggest that the directional variation of wave velocities of quartz-rich granulites do not provide the necessary impedance contrast that gives rise to strong seismic reflections.

INTRODUCTION

OVER the last 20 years, the importance of seismic anisotropy in the mantle and, more recently, in the crust has been widely discussed. Hess (1964) observed that in the upper mantle under the Pacific Ocean seismic waves travel faster perpendicular to the mid-oceanic ridge than parallel to it. Bamford (1977) and Fuchs (1979, 1983) measured strong seismic anisotropy in the subcrustal lithosphere and it is generally accepted that this observation could not be associated with lateral change in composition or physical conditions. Mantle rocks show pronounced preferred orientation of the major constituent minerals olivine (80%) and orthopyroxene (20%) (see review by Nicolas & Christensen 1987). The mantle is assumed to deform in a regime of steady-state creep in which diffusion and dislocation glide develop anisotropy during straining. Laboratory studies on representative mantle rocks led to the assumption that the olivine *a*-axis (V_{pmax} in the single crystal) is parallel to the spreading direction, whereas the olivine *b*-axis (V_{pmin} in olivine single crystal) is normal to it.

The situation in the continental crust is more complex because of vertical and lateral heterogeneities, therefore the anisotropy cannot be directly established from arrival times of seismic waves. Continental seismic reflection profiling (COCORP, DEKORP, BIRPS, ECORS, etc.) has produced a wealth of information on the structure of the continental crust. The origin of the seismic reflections in the deeper continental crust has inspired many possible explanations. In some cases, deep crustal events on seismic sections from crystalline terranes have been interpreted as originating from deep fault zones—probably mylonite zones—which have been traced to surface exposures (e.g. Brewer *et al.* 1983). The origin and preservation of subhorizontal reflectors, called lamellae, are highly debated and often attributed to: crustal laminations (e.g. Hale & Thompson 1982, Meissner 1986); compositional layering and lithologic heterogeneity (McDonough & Fountain 1988); laminated structures and anisotropy (Jones & Nur 1984; Siegesmund 1989); high pore pressures (Jones & Nur 1984) or fabric variation due to plastic deformation (Siegesmund *et al.* 1989). Up to now, it is not clear which lithological and physical properties of rocks are responsible for producing these reflecting surfaces.

The only way to test geological interpretations of deep reflection beyond the reach of the drill is the modelling

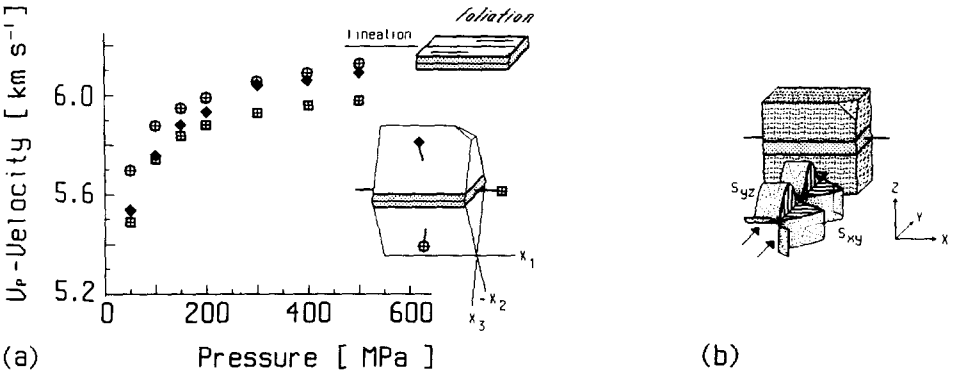

Fig. 1. Experimental results of velocity measurements. (a) Diagram of pressure dependent V_p-velocities for a cube orientation with the reference frame X_1, X_2, X_3. The planes of foliation are shaded. (b) The shaded cube gives a diagrammatic view of the orientation of the sample and the horizontally polarized shear wave (S_{xy}) and vertically polarized shear wave (S_{yz}).

of synthetic sections based on detailed geologic investigations and laboratory measurements of physical properties of rocks. One of the leading hypotheses is that anisotropic fabrics (crystallographic preferred orientation, here referred to as texture) could produce the necessary impedance contrast to cause reflecting surfaces. The correlation between preferred orientation of minerals like olivine, pyroxene, hornblende, plagioclase, phyllosilicate and the directional dependence of P- and S-wave velocities is well established (see review by Nicolas & Christensen 1987, Mainprice & Nicolas 1989, Siegesmund 1989, Siegesmund *et al.* 1989, Siegesmund & Kern 1991). However, the effect of quartz textures on the velocity anisotropy has not been investigated and a more comprehensive study of this mineral is useful because quartz is estimated to make up about 14% (volume) of the crust (Ronov & Yarozsevsky 1967). Moreover, the development of quartz textures and texture transitions have been intensively studied over the last decade (e.g. Lister 1977, Lister *et al.* 1978, review by Price 1985, Schmidt & Casey 1986, Takeshita & Wenk 1988).

In the present work, we investigate three patterns of preferred orientations of quartz: single maximum pattern, crossed-girdle texture and small-circle pattern that are commonly found in granulites (lower crustal rocks). The calculation of the elastic and seismic properties that result from the quartz textures requires the complete determination of the crystal orientation. Therefore, we developed a method which allows the direct determination of the Young's modulus from the orientation distribution function (ODF). The texture-induced directional dependence of P- and S-wave velocities and shear wave splitting for the different quartz preferred orientations will be presented and, in addition, the calculated values for a *c*-axis crossed-girdle of muscovite-bearing quartzite will be compared with the measured velocity anisotropies. Finally, we combine the calculated elastic constants derived from different quartz textures with preferred orientations of plagioclase, muscovite, orthoclase, garnet and sillimanite to estimate the seismic anisotropy of granulites from Saxony (south eastern Germany).

VELOCITY MEASUREMENTS OF V_p AND V_s AS A FUNCTION OF PRESSURE

The velocity measurements at confining pressure were carried out in a cubic pressure apparatus using the pulse transmission technique (for details see Fakhimi 1976, Kern 1982). The compressional and shear wave velocities were determined for up-pressure (room temperature) cycles measured along the three orthogonal directions (X_1, X_2, X_3) of the sample cube (Fig. 1a) which may or may not coincide with the frame of reference *XYZ* which is used here and is based on the lineation and foliation. The pressure dependence of compressional- and shear-wave velocities up to 500 MPa is only shown for V_p. The velocity increase of P-waves in the low-pressure range is associated with a progressive closure of microcracks by confining pressure (Birch 1961, Brace 1965, Christensen 1965, Siegesmund *et al.* 1991). The V_s-pressure relation (not presented here) shows the same behaviour with increasing pressure: above about 200 MPa the velocity pressure relation tends to become linear reflecting the intrinsic pressure behaviour of the crack-free material. A typical directional dependence with respect to the macroscopic fabric elements can be inferred from Fig. 1(b). The directional dependence of elastic wave velocities implies that seismic anisotropy [$A = 100(V_{pmax} - V_{pmin})/V_{pmax}$)] is a very important characteristic of crystalline rocks. Conversely, almost all rocks exhibit decreasing seismic anisotropy with increasing confining pressure particularly below 200–300 MPa. Because microcracks are closed at these pressures, the related seismic anisotropy in those rock samples results from the averaged seismic anisotropy of all constituent minerals and characterizes therefore the seismic properties of mid- and deep-crustal levels.

CALCULATION OF VELOCITY SURFACES FOR QUARTZ SINGLE CRYSTAL AND TEXTURED POLYCRYSTALS

To evaluate the elastic constants of textured polycrystals, the Voigt and Reuss averaging techniques can be

Table 1. Comparison between directional dependence of elastic wave velocities from quartz single crystal and textured polycrystals. In addition X-ray intensities are given

v [km/s] Av [%]	single crystal												textured polycrystal		
	selected crystallographic directions											all directions	single maximum	crossed girdle	small circle
hkl faces	001 c	110 a	100 m	101 r	011 z	102	012	104	014	201	021	McSkimin (1965)	Ormakan	Klamm-joch	Taylor model
v_p max												7.0	6.4	6.3	6.3
v_p min												5.3	6.0	6.0	6.0
v_p	6.4	5.8	6.0	6.0	7.1	6.4	6.9	6.4	6.6	5.5	6.8	6.29	6.21	6.19	6.19
Av_p												25	7	5	5
v_s max												5.1	4.5	4.4	4.3
v_s min												3.7	4.2	4.2	4.2
v_s	4.7	5.1	4.4	5.0	3.9	5.1	4.4	5.1	4.8	4:8	3.8	4.49	4.33	4.29	4.28
Av_s												27	6	4	2
v_{ss} max												4.7	4.3	4.3	4.3
v_{ss} min												3.2	4.0	4.1	4.1
v_{ss}	4.7	3.4	4.0	4.1	3.4	3.8	3.8	4.2	4.2	4.6	3.4	3.69	4.16	4.18	4.20
Av_{ss}												32	7	5	3
Δv_s max												1.88	0.39	0.24	0.13
Δv_s	0.1	1.8	0.6	0.9	0.6	1.4	0.7	1.0	0.6	0.3	0.6	0.80	0.17	0.12	0.08
X-ray I	<1	12	35	70+30		2+10		1+2		2+4					

applied (e.g. Bunge 1985). The calculation is carried out by averaging the elastic stiffness or compliance constants, respectively, over a distribution of grain orientations in respect of the volume fraction (e.g. Crosson & Lin 1971, Peselnick *et al.* 1974, Siegesmund *et al.* 1989). However, the preferred orientation measurements using a universal stage (U-stage) for optically uniaxial crystals, which is the case for trigonal quartz, allow only the determination of the *c*-axis. Without knowledge of the *a*-axis orientation of the individual grain, the elastic properties by Voigt and Reuss averaging is not possible. Consequently, we developed an analytical method to calculate the complete elastic properties expressing the texture by a continuous orientation distribution function (ODF). In this case the orientation information is obtained by measuring pole figures using X-ray or neutron diffraction techniques. In this study, we use the Voigt average in all calculations, because Crosson & Lin (1971) have shown that seismic P-wave velocities calculated using this technique give the closest agreement between petrofabric derived and measured seismic velocities. This is also shown quantitatively by Siegesmund (1989) with S-wave velocities and shear wave splitting.

Texture determination

The X-ray texture measurements were done with a diffraction goniometer in reflection mode using Cu(Kα) radiation. For each species, seven lattice planes (*hkl*) of quartz were measured (100, 101, 110, 111, 102, 104, 201) and necessary intensity corrections were made. The *c*-axis pattern together with *a*-, *m*- and *r*- (=*z*-) diagrams of small circle girdle are based on model data performed under low-temperature conditions (Takeshita & Wenk 1988) by a fully constrained Taylor program developed by van Houtte (personal communication) and adapted by Takeshita (1987). Further processing was done with the Gaussian peak method introduced by Wagner *et al.* (1981). The calculation of the ODF follows the mathematical method described by Bunge (1982). The texture coefficients $C_l^{\mu\nu}$ of even order (Bunge 1982) were calculated using the iterative series expansion method (Dahms & Bunge 1988, 1989) up to a degree of series expansion $L = 22$. Coincidence of the (*hkil*) and (*khil*) Bragg reflections was taken into account using intensity contribution values given by Schmid & Casey (1986). From the coefficients $C_l^{\mu\nu}$ the (001), (110), (100), (101) and (011) pole figures were recalculated (Bunge 1982).

All pole figures used in this paper and velocity diagrams have the same orientation and are given in equal-area projections (upper hemisphere). The reference frame is as follows: lineation in E–W position (*X*-direction) and foliation normal to the N–S direction (*Z*-direction) of the diagram. The *Y*-direction is normal to the lineation within the foliation plane (*XY* plane). The chosen reference frame of the single crystal ($P3_121$) coincides with that of the international tables (especially with that of fig. 1.2, p. 586, of Donnay & Le Page 1978). The *YZ* plane perpendicular to *m* includes the optic axis, the *XY* plane is perpendicular to the optic or *Z*-axis, the *XZ* plane perpendicular to these two planes includes the two-fold *a*. To present the elastic properties, Johnson & Wenk (1986) used a reference frame which is rotated 90° anticlockwise to the system used here which describes crystal faces. For an easier comparison between single crystal directions and the respective directions in the polycrystalline aggregate, we used a uniform reference system for faces and velocities.

Single crystal anisotropy

Before considering the directional dependence of elastic wave velocities of polycrystals, it is useful to investigate the properties of the single crystal (Table 1). The directional dependence of elastic wave velocities for V_p, V_s (faster S-wave) and V_{ss} (slower S-wave, perpendicularly polarized to V_s) in a quartz single crystal is shown in Figs. 2(a)–(d). The complete description of the

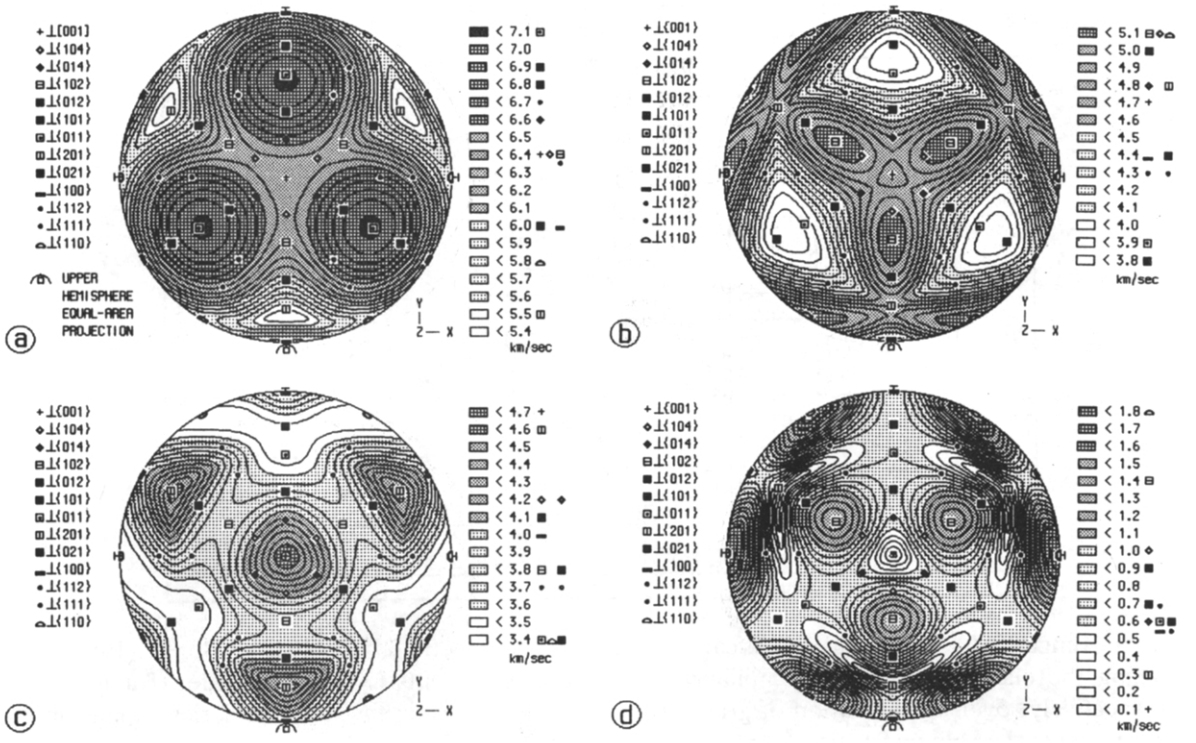

Fig. 2. Single crystal velocities of quartz. Braces {*hkl*} enclose all crystallographic equivalent faces or sets of lattice planes of a special form (*hkl*) with the reciprocal axis intercepts *h*, *k*, *l*. Symbol (inverted T) before brace indicates a normal direction to (*hkl*). Contours at 100 m s^{-1} intervals. (a) P-waves V_p. (b) Faster S-waves V_s. (c) Slower S-waves V_{ss}, (d) Shear wave splitting ΔV_s.

elastic properties of the trigonal quartz requires six independent elastic constants (McSkimin *et al.* 1965). The velocity surfaces (equal-area projections, upper hemisphere) in Fig. 2 are oriented with respect to the hexagonal (trigonal) standard crystal orientation projection. The velocity diagrams illustrate the single threefold symmetry axis characteristic of the trigonal crystal symmetry of quartz. The single crystal velocities are plotted together with the most important crystal directions.

The maximum of P-wave velocities (V_{pmax}) is approximately normal to *z*-rhombohedral faces, intermediate V_p is parallel to the *c*-axis and V_{pmin} is approximately normal to the {201}-planes. The fastest V_s is observed to be parallel to the *a*-axes and approximately normal to *r*, the slowest V_s is approximately normal to the *r*-rhombohedron. The slower shear wave V_{ss} has the fastest velocity parallel to the *c*-axis and slowest approximately normal to *r* and {201}-planes and *a*. As can be seen in Fig. 2(d), there is a pronounced shear wave splitting in the quartz single crystal. According to the trigonal crystal symmetry, there is no acoustic birefringence parallel to the *c*-axis. The anisotropy reaches values of V_p: 25%, V_s: 27% and V_{ss}: 32%. The mean velocities are V_p: 6.29 km s^{-1}, V_s: 4.49 km s^{-1} and V_{ss}: 3.69 km s^{-1}.

Determination of the elastic constants from the ODF

The elastic constants $\bar{C}_{mnop}$ of a polycrystalline aggregate can be calculated from the texture coefficients $C_l^{\mu\nu}$ by Bunge (1982, 1985):

$$\bar{C}_{mnop} = \sum_{l=0(2)}^{4} \sum_{\mu=1}^{M(l)} \sum_{\nu=1}^{N(l)} \frac{1}{2l+1} C_l^{\mu\nu} a_l^{\mu\nu}(mnop). \quad (1)$$

The coefficients $a_l^{\mu\nu}(mnop)$, respectively, can be understood as series terms describing the single crystal elastic constants. It is:

$$a_l^{\mu\nu}(mnop) = (2l+1) \oint \sum_{i=1}^{3}\sum_{j=1}^{3}\sum_{k=1}^{3}\sum_{l=1}^{3} \times g_{im} g_{jn} g_{ko} g_{lp} C_{ijkl} \dot{T}_l^{\mu\nu}(g)\, dg. \quad (2)$$

Here, C_{ijkl} are the usual elastic constants, the functions $\dot{T}_l^{\mu\nu}$ are symmetric generalized spherical harmonics. The integration is carried out over all possible orientations *g*,

Fig. 3. Texture diagrams (type single maximum) of the Ormakam quartzite (Stavanger area, Norway) which were done by ODF recalculation. Sets of lattice planes are indicated by a common letter which is used for both, faces (*m*, *r*, *z*: crystallographic planes) and the axes (*c* and *a*) normal to these planes and by a special form symbol (*hkl*). (a)–(e) Contours: 1, 3, 5, 7, 9 and 11 multiple random distribution (m.r.d.). (a) {001}. (b) {110}. (c) {100}. (d) {101}. (e) {011}. (f)–(i) Velocities calculated using elastic properties from ODF: (f) V_p; (g) V_s; (h) V_{ss}; (i) ΔV_s. (j) Texture diagram of $\{101\}_{70\%} + \{011\}_{30\%}$ measured with X-rays.

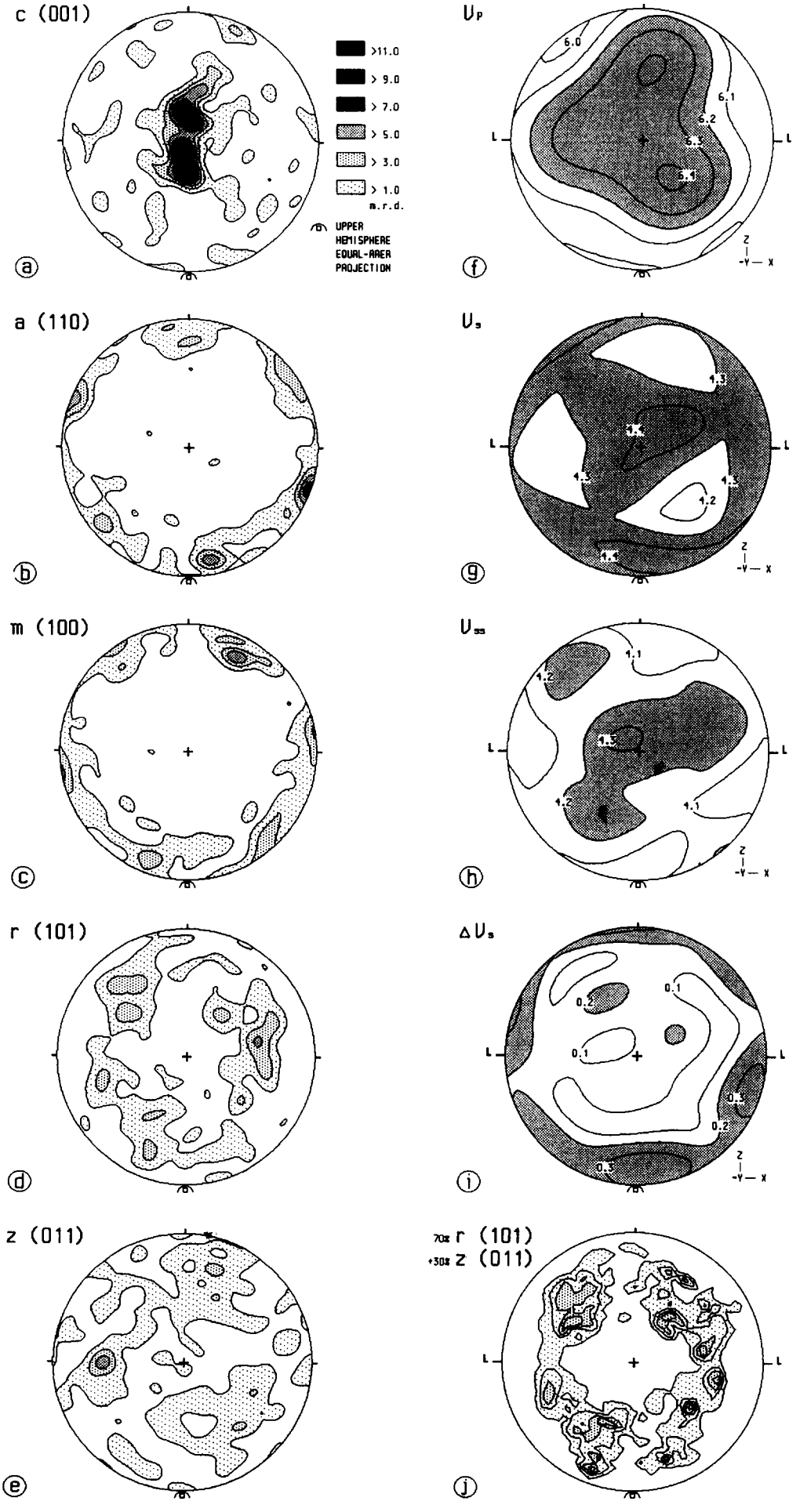
c (001)
>11.0
> 9.0
> 7.0
> 5.0
> 3.0
> 1.0
m.r.d.
UPPER HEMISPHERE EQUAL-AREA PROJECTION
a
a (110)
b
m (100)
c
r (101)
d
z (011)
e
Vp
6.0
6.1
6.2
6.3
6.4
f
Vs
1.3
1.4
1.5
1.2
1.1
g
Vss
1.1
1.2
1.3
1.2
1.1
h
ΔVs
0.2
0.1
0.1
0.3
0.2
0.3
i
70% r (101)
+30% z (011)
j
L
Z
-Y — X

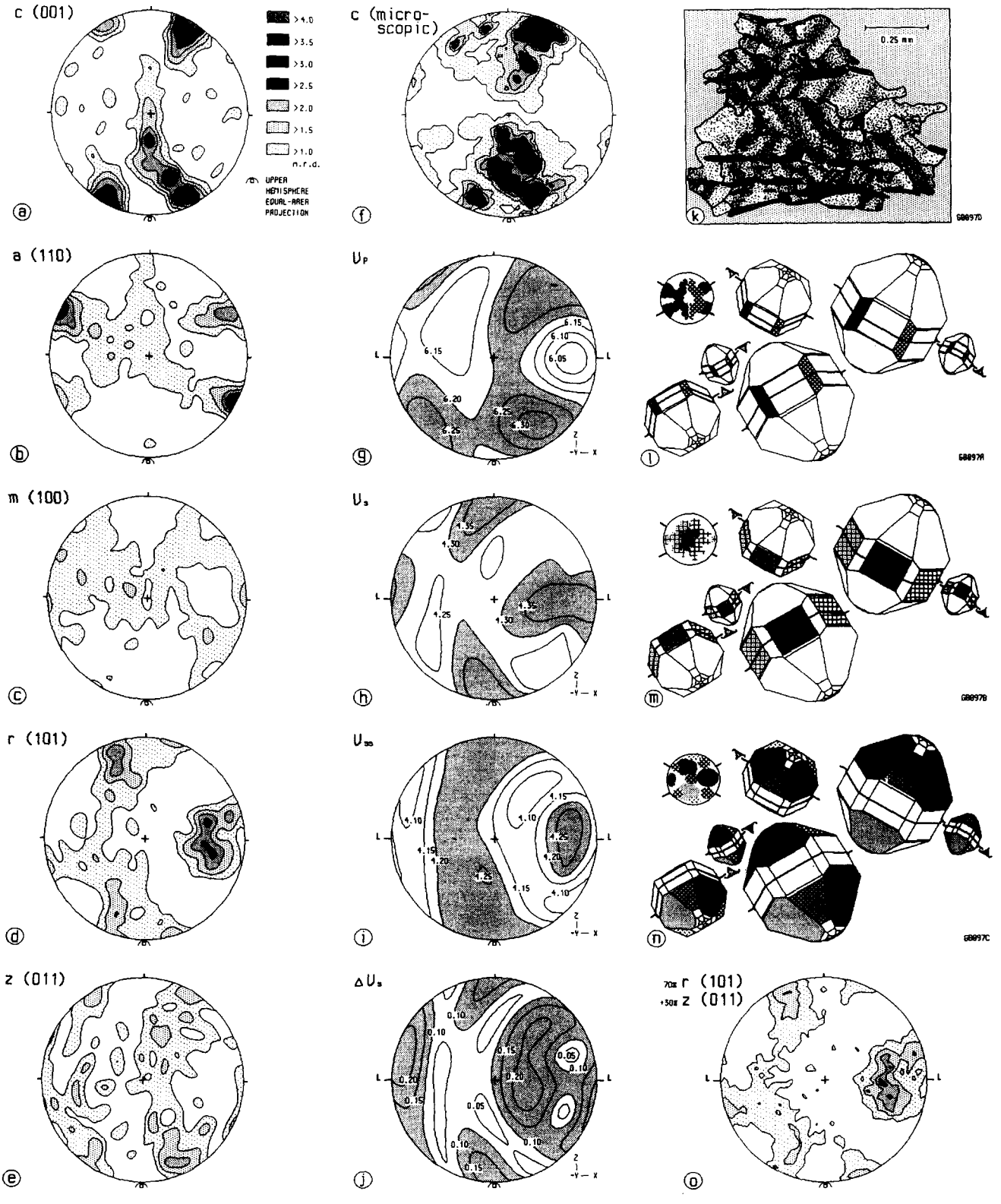

Fig. 4. Texture diagrams (type cross-girdle) of Klammljoch quartzite (Bruneck area, Italy) were done by ODF recalculation for sets of lattice planes indicated by a letter and a special form (*hkl*). (a)–(d) Contours: 1.0, 1.4, 1.8, 2.2, 2.6, 3.0 and 3.4 m.r.d. (a) {001}. (b) {110}. (c) {100}. (d) {101}. (e) {011}. (f) Universal stage measurements of *c*-axes; contours: 1, 2, 3, 5, 7 and 10 m.r.d. (g)–(j) Velocities calculated using elastic properties from ODF: (g) V_p; (h) V_s; (i) V_{ss}; (j) ΔV_s. (k) Sketch of part of a thin section showing undulatory extinction of quartz (stippled) and muscovite (dark lined). (l)–(n) Pseudo-quartz crystals which summarize the main quartz fabric: size is proportional orientation frequency; darker patterned parts indicate the main lattice plane orientations; face area is proportional X-ray intensity. (l) {110}. (m) {100}. (n) {101}. (o) Texture diagram of $\{101\}_{70\%} + \{011\}_{30\%}$ measured with X-rays.

and $g_{im}, \ldots, g_{lp}$ represent components of the orientation matrix (Bunge 1982).

Equation (2) can be solved in two ways. The more correct way is to solve equation (2) analytically. This has been done for orthorhombic and higher symmetries by Morris (1969). It is clear that equation (2) then decomposes into purely mathematical quantities and the components of the elastic tensor. Johnson & Wenk (1986)

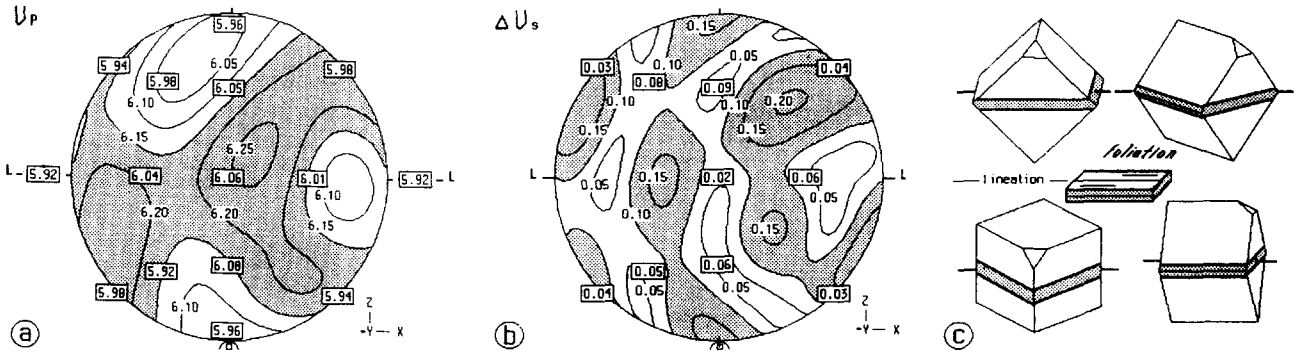

Fig. 5. Experimental and theoretical results. (a) Measurements at 400 MPa for V_p (boxes) together with calculated values (velocity contours) of V_p for a sample (97% quartz, 3% muscovite). (b) Measurements at 400 MPa for ΔV_s (boxes) and calculated values (velocity contours) of ΔV_s of the same sample. (c) Four views of cubic samples showing lineation and planes of foliation that were used in the experiments.

applied this to predict the elastic anisotropy of a polycrystalline calcite aggregate. With respect to sample symmetry, their synthetic texture was orthorhombic. Because of that they could treat crystal symmetry as quasi-hexagonal. Hence they were able to directly apply Morris' formalism to their problem. In our case of a trigonal crystal and triclinic sample symmetry, equation (2) is solved numerically in steps of 5° through the whole asymmetric unit of the Euler space. This procedure is carried out once for each possible combination of the parameters l, μ, ν, m, n, o, p. The series coefficients are stored for the case of quartz. They can easily be calculated again for other materials independent of crystal and sample symmetries if the elastic tensor C_{ijkl} is known. Hence, the present method accounts for trigonal crystal symmetry in quartz, and the procedure is valid for any crystal symmetry. It is not necessary to account for the lack of centrosymmetry in quartz (i.e. enantiomorphism). Both seismic and X-ray measurements physically 'add' a centre of inversion to the crystal, which results in the fact that only even orders of series expansion are to be considered.

QUARTZ TEXTURES OF EXAMPLE GRANULITES AND THEIR SEISMIC PROPERTIES

We have attempted to test the effects of quartz fabric anisotropy on the seismic velocities for granulites and associated gneisses from Saxony (south-central Germany) which are intensively studied (Behr 1961, 1968, Lister & Dornsiepen 1982). In these high-grade metamorphic rocks, quartz shows three main types of orientation on *c*-axis diagrams: (1) crossed-girdle patterns parallel to the foliation in the interior of the granulite complex; (2) crossed-girdles at the deformed margins of the complex; and (3) a single maximum pattern at the mylonitized extreme margins of the granulites. These orientation patterns are observed to grade into one another; this feature was also observed in the Tirschheim borehole sample by Behr (1961).

The method discussed here as well as the quartz anisotropy effects would best be tested directly by comparison of calculated and measured seismic velocities in real granulites. However, the X-ray texture measurements, which are necessary to carry out the velocity calculation, cannot presently be successfully performed on polyphase rocks (e.g. granulites). As an alternative, we measured samples from other areas that show similar *c*-axis diagrams and used a data set calculated after Takeshita & Wenk (1988). From the two measured examples, six pole figures were obtained, which allowed the calculation of the ODF. The anisotropy of quartz that is based on these values was used along with data for the other constituent minerals of the Saxonian granulites to calculate anisotropy values for the whole rocks. As an actual comparison of the calculated and measured anisotropies a muscovite-bearing quartzite was used.

Single maximum pattern

The fine-grained quartzite (Ormakam-area, NE Stavanger, Norway) is dynamically recrystallized (0.2–0.6 mm) and contains only 0.2 volume per cent muscovite. The *c*-axes (Fig. 3a) are concentrated (>11 m.r.d., i.e. multiple random distribution) at the centre of the diagram (Y) forming a double maximum including a solid angle of 20°. The lineation (X) seems to be the rotation axis. The *c*-axes orientation pattern of the specimen investigated in this study is similar to that (diagram D, p. 133) of Müller & Wurm (1969). They describe the quartzite as narrowly folded around an older *b*-axis (fold axes). The (110)-concentrations (*a*-axis diagram) lie near the primitive circle (Fig. 3b). A similar pattern—solid angles to maxima of (110) are about 30°—is observed for the (100)-reflection (Fig. 3c). Each set of submaxima of the {101} (Fig. 3d) and {011} (Fig. 3e) lattice planes have a three-fold symmetry—solid angles of (101)-maxima to (011)-maxima 60°. The similarity to the single crystal pattern is striking.

Calculated P- and S-wave velocities of c-axis single maximum pattern

The diagrams of the P- and S-wave velocities (Figs. 3f–i) correspond to the texture (Figs. 3a–e) and have the same three-fold symmetry axis near the centre (tilted some degrees towards NW) as single crystals. The de-

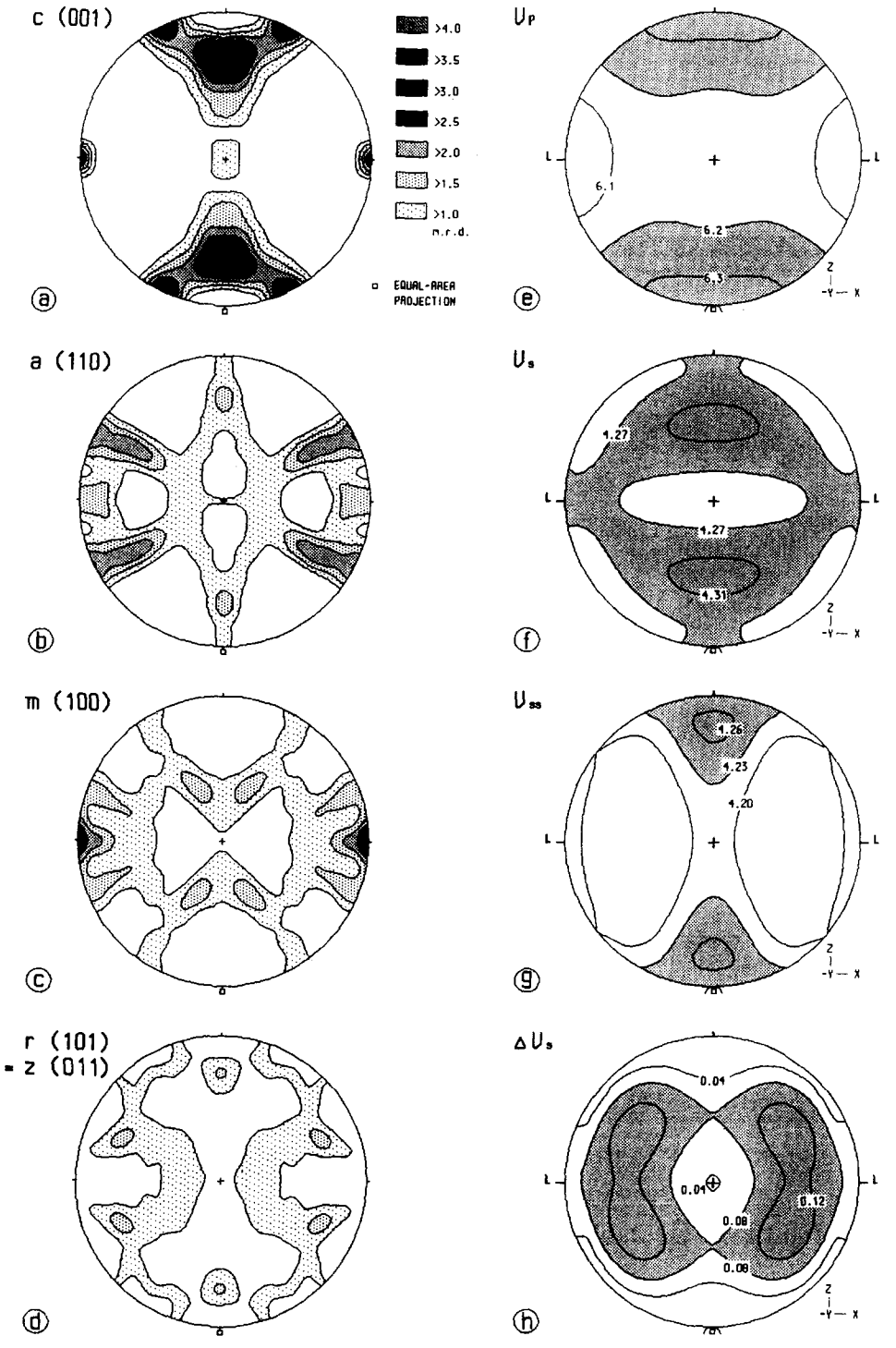

Fig. 6. Texture diagrams (type small-circle girdle) showing calculated quartz orientations (Taylor method); the ODF recalculations were done for sets of lattice planes which are indicated by a letter and a special form (*hkl*). (a)–(d) Contours: 1, 3, 5, 7, 9 and 11 m.r.d. (a) {001}. (b) {110}. (c) {100}. (d) {101} = {011}. (e)–(h) Velocities calculated using elastic properties from ODF: (e) V_p; (f) V_s; (g) V_{ss}; (h) ΔV_s. See also the caption of Fig. 2.

scription can be concisely referred back to single crystal velocities (Fig. 2) by clockwise rotation of 90°. As seen in Table 1, mainly the velocity anisotropy [*A*] is reduced for V_p: 25 to 7%, V_s: 27 to 7% and V_{ss}: 32 to 7%. The similarity of position of *r*-maxima (Fig. 3d, also measurements Fig. 3j) and V_{ss}-maxima (Fig. 3h) and also of *z*-maxima (Fig. 3e) and V_p-maxima (Fig. 3f) is distinct. The difference between the two shear waves (shear wave splitting, Fig. 3i) is highest along a zone almost normal to *Y* (−*Y* in the upper hemisphere for having a right-handed reference frame). This zone can be referred to the *a*-maxima (Fig. 3b).

Crossed-girdle pattern

This quartzite (Klammljoch, E-Bruneck, Austria) belongs to a sequence of Triassic sediments from the "Matreier Zone" metamorphosed at greenschist facies conditions. The rock exhibits a pronounced foliation

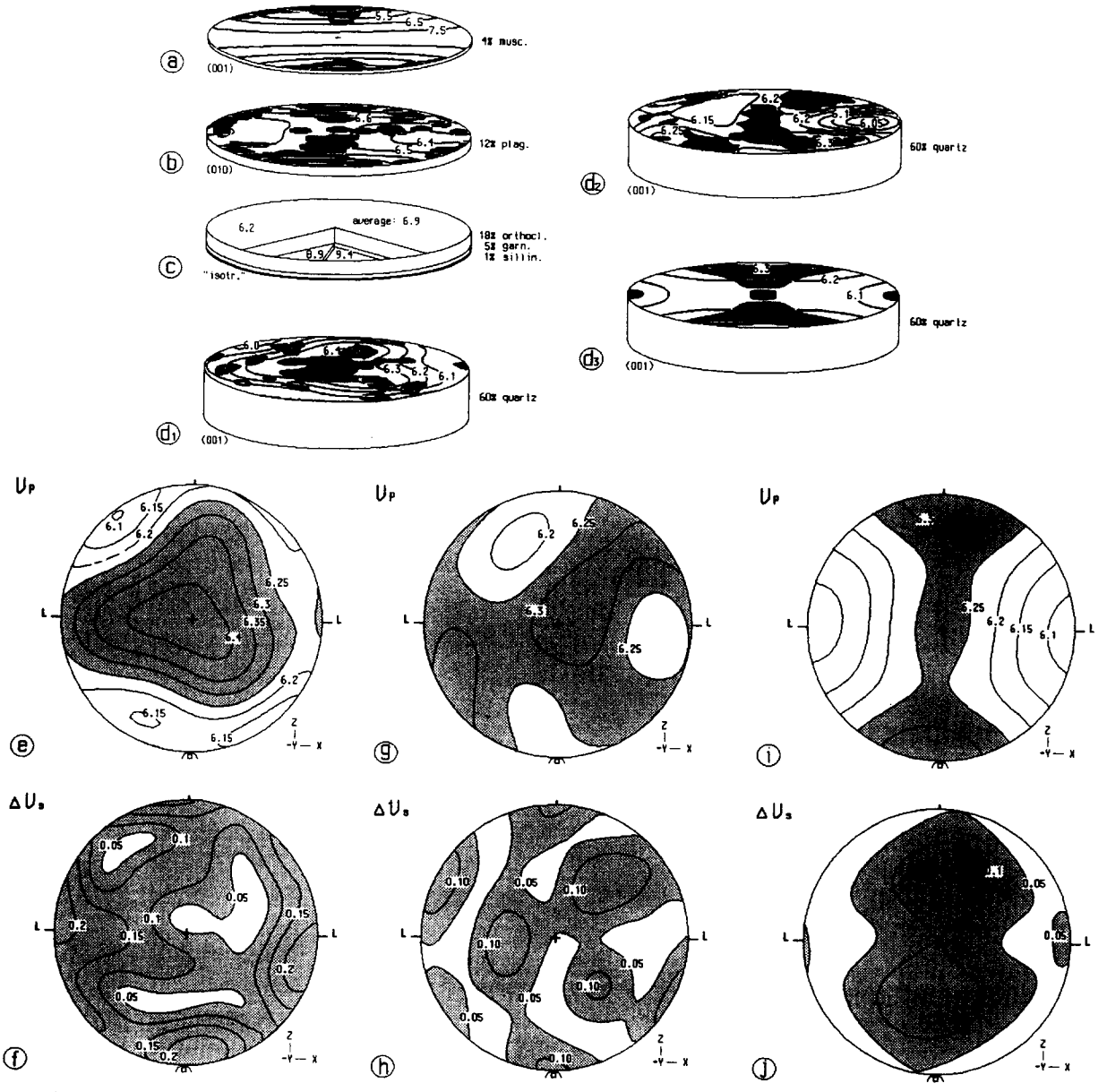

Fig. 7. Model granulites. For (a), (b), (c), (d_1), (d_2) and (d_3) thickness of diagram discs correspond to modal proportions of minerals; preferred orientations of selected sets of lattice planes (indices = *hkl*) are shown by the filled areas; contour lines indicate equal V_p-velocities (km s^{-1}) and represent each mineral's contribution to seismic anisotropy of the sample. (e)–(f), (g)–(h), and (i)–(j) are calculated V_p and ΔV_s values for the three samples and are derived from: I, (a)–(d_1); II, (a)–(c) & (d_2); and III, (a)–(c) & (d_3).

with the *s*-planes dipping steeply to the south and is accentuated by muscovite crystals (about 5 vol.-%). The microstructure is illustrated in the idealized thin section sketch (Fig. 4k) where two sets of grains distinguished by different undulatory extinction are seen together with muscovite. Each direction of extinction coincides with the respective *c*-axes zones of Fig. 4(f). The *c*-axes (Figs. 4 a & f) form an incomplete crossed-girdle with two main maxima at the primitive circle (solid angle +30° and −30° from *Z*, the normal to foliation plane *XY*). The *a*-diagram (Fig. 4b) has also two main maxima at the primitive circle (solid angle +30° and −30° off to the lineation (*X*), the *r*-diagram (Fig. 4d) a main maximum in *XY* (solid angle −30° off to *X*) and two at a girdle (solid angle −120° from *X*) and the *z*-diagram (Fig. 4e) some maxima at a small circle (two parts, −60° and −150° from *X*). The *m*-diagram (Fig. 4c) has only a weak preferred orientation.

The texture can be geometrically illustrated by six crystals with selected orientations (Figs. 4l–n) which was also done in a schematically reduced form by Schmid & Casey (1986). In our case, the crystals represent the main averaged orientations of the quartz texture, the volumes of the crystals are proportional to the grain frequency, and the sizes of the faces of each crystal are proportional to the X-ray intensity (Table 1). Measured and recalculated pole figures are in good agreement. As a measure of the agreement, we compared a recalculated *c*-axes pole figure, which cannot be directly measured with X-rays, with a *c*-axes diagram measured with a U-stage (Figs. 4a & f) and the recalculated (101) with the measured $(101)_{70\%} + (011)_{30\%}$ diagram, which

contains 2.3 times more {101} than {011} (Fig. 4o). This diagram gives directly (for the faster shear wave together with the *a*-diagram) a rough notion of shear wave maxima.

Calculated P- and S-wave velocities of c*-axis crossed-girdle pattern*

The velocity diagrams (Figs. 4g–j) are estimated with ODF calculations but can be understood also with the aid of the fabric diagrams (Figs. 4a–e), the six crystals (Figs. 4l–n), the single crystal velocities (Fig. 2) and Table 1. The velocity anisotropy is reduced with respect to the single maximum sample. The ideal maximum anisotropy would be found in single oriented crystals, for V_p: 25%, V_s: 27% and V_{ss}: 32%, and the maximum shear wave splitting would be 1.88 km s^{-1}. In rocks, as already shown for the case of a single maximum, the anisotropy will be less pronounced: for the crossed-girdle sample these changes in velocities give values for V_p: 5%, V_s: 4% and V_{ss}: 5% and shear wave splitting reaches 0.24 km s^{-1}.

Comparison of calculated texture based and measured velocity anisotropy

In order to demonstrate the velocity variation of this muscovite-bearing quartzite based on the crystallographic orientation of the component minerals (quartz [95 vol.-%], muscovite [5 vol.-%]), we calculated the aggregate elastic constants (Voigt average) and determined the seismic velocities by solution of the Christoffel equation (Crosson & Lin 1971). The single-crystal elastic constant for muscovite were taken from Belikov *et al.* (1970). In order to estimate the anisotropy contribution of each mineral to the total velocity anisotropy, we use as a simple case two components, quartz and muscovite. The experimental data (boxes) and the calculated values (velocity contours) are given in Figs. 5 (a) & (b). The directional dependence of the P-wave velocities of the measured (shown by the orientation of sample cubes in Fig. 5c) and calculated values generally agree. The ΔV_s-diagrams also coincide in all directions. The observed difference in the absolute velocity values (Fig. 5a) may be attributed to the assumptions of constant elastic strain and zero porosity. Secondly, the volume fraction of muscovite may differ and its preferred orientation may also vary in the sample cubes that were investigated. The single crystal velocity anisotropy of muscovite is high and the *c*-axes are preferentially oriented (V_p minimum in the single crystal) normal to foliation. Therefore, small differences in the relative volume content would considerably modify the whole rock anisotropy.

Small circle pattern

The *c*-axis pattern together with *a*-, *m*- and *r*- (=*z*-) diagrams of small circle girdle are based on model data calculated with the Taylor model and assuming low-temperature conditions (Takeshita & Wenk 1988). These data provide a small circle pattern, which is additionally highly symmetric. The two main maxima of model quartz *c* (Fig. 6a) near *Z* are close together in a small circle zone, one in the upper and one in the lower half of the diagram. Two weaker maxima in the same zone lie at the primitive circle and a very weak one (two parts) at the lineation points. The *a*-, *m*-patterns (Figs. 6 b & c) deviate more or less from that of natural samples, the *r*-pattern (Fig. 6d) is methodically the same as the *z*-pattern which is not observed for the two natural samples.

Calculated P- and S-wave velocities of c*-axis small circle pattern*

The velocities of the small circle patterns (Figs. 6e–h) are similar to those of the crossed-girdle (Figs. 4g–j) and can be seen also in Table 1. The crossed-girdle is incomplete, but the texture is quite similar to the small circle texture if one does not take into account the asymmetric form of crossed-girdle. The main differences are lower shear velocities (Figs. 6f & g) near the lineation axis *X* and lower values for shear wave splitting (Fig. 6h) near *Z* and at the position of main *a*-axes (Fig. 6b). The anisotropy is less pronounced for shear waves (Av_s: 2%, Av_{ss}: 3%) and the bulk shear wave splitting has only two-thirds that of the crossed-girdle.

Calculated velocity anisotropy of 'Saxonian' granulites

To demonstrate the effect of different quartz orientations (Figs. $7d_1$, d_2 & d_3; *c*-axes are labelled in black) on the directional dependence of elastic wave velocities of any rock composition, we combined the respective elastic constants with those of plagioclase, orthoclase, muscovite, garnet and sillimanite. We chose three lower crustal granulites from the Saxony terrain (granulites I, II and III) with an average mode of 60% quartz, 18% perthitic feldspar, 12% plagioclase, 5% garnet, 4% muscovite and 1% sillimanite (Figs. 7a–d). In this area the texture transition from small-circle girdle *c*-axes distribution (granulite III, Fig. $7d_3$) around the outer borders of the Saxonian granulite complex to crossed-girdle pattern (granulite II, Fig. $7d_2$) in the core of the complex was reported by Behr (1968). In addition, single maximum *c*-axes pattern (granulite I, Fig. $7d_1$) are also observed. These three types of *c*-axes patterns are used to model the granulites I (Figs. $7d_1$–f), II (Figs. $7d_2$, g & h) and III (Figs. $7d_3$, i & j). Except for quartz orientation the texture of the other minerals is identical in all calculated samples (Figs. 7a–c). For plagioclase and muscovite, we used commonly reported mineral textures with the (010) normals (V_{pmax} of the plagioclase single crystal) perpendicular to the foliation (Fig. 7b) and poles normal to (001) (V_{pmin} of muscovite single crystal) perpendicular to foliation (Fig. 7a). The perthitic feldspar is assumed to be orthoclase and randomly distributed (Fig. 7c), which, according to Behr (1961), is

realistic. In addition to orthoclase, the garnet and sillimanite is also assumed to be randomly distributed. The calculated velocity anisotropies for P-waves of our granulites I, II and III are 5, 3 and 1%. The differences in the shear-wave velocities (ΔV_s) are 0.29, 0.14 and 0.14 km s^{-1}, respectively. The P- and S-wave velocities of the three granulites vary between 6.08 and 6.43, and 3.86 and 4.10 km s^{-1}. The V_p-values are low in comparison to those commonly reported from lower crustal seismic records, but in agreement with the experimental data on felsic granulites from Calabria (Kern & Schenk 1988).

The single crystal anisotropy for V_p and V_s of quartz (25%, 27%), plagioclase (24%, 29%) and muscovite (45%, 53%) are high; whereas, the contribution of orthoclase, garnet and sillimanite is isotropic in the model. The interaction of the calculated texture-based velocities of the various mineral phases illustrates the complex nature of the whole rock velocity anisotropy. For example, in granulite I (Fig. 7e), in addition to the isotropic contribution of orthoclase, garnet and sillimanite the texture-related velocity anisotropy (V_p) of plagioclase (7%), muscovite (40%) and quartz (7%) give only 5% anisotropy of the whole rock. The superposition of the velocities of the strong preferred oriented minerals (plagioclase, Fig. 7b; muscovite, Fig. 7a; quartz, Fig. 7d$_1$) reduces the V_p-anisotropy of the investigated model rock (Fig. 7e) in relation to the volume fraction of each mineral.

DISCUSSION

The seismic layering of the lower crust is a common feature in Hercynian and Caledonian consolidated continental crust, and is characterized by a strong and laterally consistent layering with alternating high and low P-wave velocities (e.g. Meissner 1986). Lithological interpretation of the observed seismic laminations involve compositional layering, magmatic differentiation, partial melting, fluid enrichment, mylonite zones and anisotropy. Anisotropy may be of importance with respect to the seismic phenomena commonly reported from the lower continental crust. Taking our granulites, assuming horizontal layering from granulite I to granulite III, and using Z as the propagation direction (normal to the foliation and lineation), we obtain reflection coefficients (R_c) for V_p at the interfaces of 0.003 and 0.009. The R_c for the two perpendicular polarized shear waves (V_s, V_{ss}) are, respectively, 0.010, 0.013 and −0.001, −0.004. Alone these texture-related values should not give seismic reflections without a complementary change in composition. Strong seismic reflections can be observed for R_cs around 0.1 (Meissner 1986, McDonough & Fountain 1988) or R_cs of 0.03–0.05 where the layer thickness is 100 m induced by constructive interferences. Our low reflection coefficients suggest, that the anisotropy of the felsic granulites with strong quartz, feldspar and muscovite textures cannot explain the seismic layering at deeper crustal levels.

A deep crustal profile which crosses the Saxony granulites (Bölsche & Kresser 1978) shows that the lower crust is more reflective than the upper crust. Since our estimated reflection coefficients due to the strain-induced quartz texture of the felsic granulites are low, a lithological contrast (density-related impedance contrast) between the felsic granulites and the intercalated pyriclasites would be a more realistic cause for producing reflecting surfaces (see also Fountain & Burke 1990). Specifically, in rocks with high velocity minerals and high seismic anisotropy (e.g. amphibole, pyroxene, sillimanite, garnet, etc.) the influence of quartz textures should be of minor importance.

To correctly diagnose the meaning and significance of the seismic records a closer liaison between structural geology, petrophysics and geophysics should offer a better understanding of the relationship between anisotropic fabric, anisotropic physical properties and their geophysical expression. More work on the relationship between texture-induced anisotropy, compositional layering and seismic modelling for P- and S-wave velocities (e.g. Lüschen *et al.* 1990: Siegesmund *et al.* submitted) using cross sections examined by structural geologists are necessary to explain the seismic nature of the lower crust in terms of lithological and physical rock properties.

Acknowledgements—We thank H. Kern (Kiel) for the permission to do a few measurements with the cubic pressure apparatus of the institute and T. Takeshita (Matsuyama) for making available the adapted Taylor model computer code of P. van Houtte (Leuven), who gave his permission for its use. We are especially thankful to O. Mehlberg and the computer science students employed in the Mineralogy Institute at Kiel, K. Hoppe and A. Wacknitz, who on their own time helped salvage essential data from a dying hard disk.

REFERENCES

Bamford, D. 1977. P velocity anisotropy in a continental upper mantle. *Geophys. J.* **49**, 29–48.

Behr, H.-J. 1961. Beiträge zur petrographischen und tektonischen Analyse des sächsischen Granulitgebirges. *Freiberger Forsch.* **C119**, 5–118.

Behr, H.-J. 1968. Zur tektonischen Analyse magmatischer Körper unter besonderer Berücksichtigung des Quarz Kornefüges II. *Freiberger Forsch.* **C29**, 33–98.

Belikov, P., Alexandrov, K. C. & Ryshova, T. V. 1970. *Elastic Properties of Rock-forming Minerals and Rocks.* Nauka, Moscow.

Birch, F. 1961. The velocity of compressional waves in rocks to 10 kilobars, 2. *J. geophys. Res.* **66**, 2199–2224.

Bölsche, J. & Kresser, K. D. 1978. First results of depth seismic exploration in the southern part of G.D.R. In: *Proc. XXII Int. Geophys. Symp. 1977*, Prague, **1**, 457–472.

Brace, W. F. 1965. Some new measurements of linear compressibility of rocks. *J. geophys. Res.* **70**, 391–398.

Brewer, J., Matthews, D., Warner, N., Hall, J., Smythe, D. & Wittington, R. 1983. Birps deep seismic reflection studies of the British Caledonides. *Nature* **305**, 205–210.

Bunge, H. J. 1982. *Texture Analysis in Materials Sciences.* Butterworth, London.

Bunge, H. J. 1985. Physical properties of polycrystals. In: *Preferred Orientation in Deformed Metals and Rocks: An Introduction to Modern Texture Analysis* (edited by H.-R. Wenk). Academic Press, Orlando, 507–525.

Christensen, N. I. 1965. Compressional wave velocities in metamorphic rocks at pressures to 10 kilobars. *J. geophys. Res.* **70**, 6147–6164.

Crosson, R. S. & Lin, J. W. 1971. Voigt and Reuss prediction of anisotropic elasticity of olivine. *J. geophys. Res.* **76**, 570–578.

Dahms, M. & Bunge, H. J. 1988. ODF calculation by series expansion from incompletely measured pole figures using the positive condition—Part II. All crystal symmetries. *Textures & Microstruct.* **8/9**, 97–114.

Dahms, M. & Bunge, H. J. 1989. The iterative series-expansion method for quantitative texture analysis. I. General outline. *J. appl. Cryst.* **22**, 439–447.

Donnay, J. D. H. & Le Page, Y. 1978. The vicissitudes of the low-quartz crystal setting or the pitfalls of enantiomorphism. *Acta Cryst.* **A34**, 584–594.

Fakhimi, M. 1976. Interpretation seismischer Krustenmessungen aufgrund des Geschwindigkeitsverhaltens charakteristischer Gesteine bei Hochdruck- und Hochtemperaturversuchen am Beispiel von Ivrea. Unpublished Ph.D. thesis, Universität Kiel.

Fountain, D. M. & Burke, M. 1990. Seismic properties of rocks from an exposure of extended continental crust—new laboratory measurements from the Ivrea Zone. *Tectonophysics* **182**, 119–146.

Fuchs, K. 1979. The subcrustal lithosphere—mechanical properties, differentiation and dynamical processes. *Tectonophysics* **56**, 1–15.

Fuchs, K. 1983. Recently formed elastic anisotropy and petrological models for the continental subcrustal lithosphere in southern Germany. *Phys. Earth & Planet. Interiors* **31**, 93–118.

Hale, L. D. & Thompson, G. A. 1982. The seismic reflection character of the continental Mohorovicic discontinuity. *J. geophys. Res.* **87**, 4625–4635.

Hess, H. H. 1864. Seismic anisotropy of the uppermost mantle under oceans. *Nature* **203**, 629–631.

Jones, T. & Nur, A. 1984. The Nature of seismic reflections from deep crustal fault zones. *J. geophys. Res.* **89**, 3153–3171.

Johnson, G. C. & Wenk, H.-R. 1986. Elastic properties of polycrystals with trigonal crystal and orthorhombic specimen symmetry. *J. appl. Phys.* **60**, 3868–3875.

Kern, H. 1982. P- and S-wave velocities in crustal and mantle rocks under the simultaneous action of high confining pressure and high temperature and the effect of the rock microstructure. In: *High-pressure Researches in Geosciences* (edited by Schreyer, W.). Schweitzerbartsche, Stuttgart, 15–45.

Kern, H. & Schenk, V. 1988. A model of velocity structure beneath Calabria, Southern Italy, based on laboratory data. *Phys. Earth & Planet. Int. Sci. Lett.* **87**, 325–337.

Lister, G. S. 1977. Discussion. Crossed-girdle *c*-axis fabrics in quartzites plastically deformed by plane strain and progressive simple shear. *Tectonophysics* **34**, 91–99.

Lister, G. S. & Dornsiepen, U. F. 1982. Fabric transitions in the Saxony granulite terrain. *J. Struct. Geol.* **4**, 81–92.

Lister, G. S., Paterson, M. S. & Hobbs, B. E. 1978. The simulation of fabric development during plastic deformation and its application to quartzite: The model. *Tectonophysics* **45**, 107–158.

Lüschen, E., Nolte, B. & Fuchs, K. 1990. Shear wave evidence for an anisotropic low crust beneath the Black Forest, southwest Germany. *Tectonophysics* **173**, 483–493.

Mainprice, D. & Nicolas, A. 1989. Development of shape and lattice preferred orientation: application to the seismic anisotropy of the lower continental crust. *J. Struct. Geol.* **11**, 179–189.

McDonough, D. T. & Fountain, D. M. 1988. Reflection characteristics of a mylonite zone based on compressional wave velocities of rock samples. *Geophys. J.* **93**, 547–558.

McSkimin, H. J., Anreatch, P., Jr & Thurston, R. N. 1965. Elastic moduli of quartz versus hydrostatic pressure at 25 and −195.8°C. *J. appl. Phys.* **36**, 1624–1632.

Meissner, R. 1986. The continental crust—a geophysical approach. *International Geophysics Series, Vol.* 34. Academic Press, Orlando.

Morris, P. R. 1969. Averaging fourth-rank tensor with weight functions. *J. appl. Phys.* **40**, 447–448.

Müller, G. & Wurm, F. 1969. Die Gesteine der Inselgruppe Randöy-Fogn. Beiträge zur Metamorphose und zum Aufbau der kambro-silurischen Gesteine des Stavanger—Gebietes I. *Norsk. geol. Tidsskr.* **49**, 97–144.

Müller, G. & Wurm, F. 1970. Die Gesteine der Halbinsel Strand. Beiträge zur Metamorphose und zum Aufbau dert kambrosilurischen Gesteine des Stavanger—Gebietes II. *Norges geol. Undersök.* **267**, 1–58.

Nicolas, A. & Christensen, N. L. 1987. Formation of anisotropy in upper mantle peridotites—a review. *Rev. Geophys.* **25**, 111–123.

Peselnick, L., Nicolas, A. & Stevenson, P. R. 1974. Velocity anisotropy in a mantle peridotite from the Ivrea Zone: Application to upper mantle anisotropy. *J. geophys. Res.* **79**, 1175–1182.

Price, G. P. 1985. Preferred orientation in quartzites. In: *Preferred Orientation in Deformed Metals and Rocks: An Introduction to Modern Texture Analysis* (edited by Wenk, H.-R.). Academic Press, Orlando, 385–406.

Ronov, A. V. & Yarozsevsky, A. A. 1967. Chemical composition of the earth's crust. *Geochimija* **11**, 1285–1309.

Schmid, S. M. & Casey, M. 1986. Complete fabric analysis of some commonly observed quartz *c*-axis patterns. *Am. Geophys. Un. Geophys. Monogr.* **36**, 263–286.

Siegesmund, S. 1989. Texturelle und strukturelle Eigenschaften mylonitischer Gesteine der Insubrischen Linie (Ivrea-Zone, Italien) und ihr Einfluß auf die elastischen Gesteinseigenschaften. Ein Beitrag zur Interpretation seismischer *in situ*-Messungen. Unpublished Ph.D. thesis, Universität Kiel.

Siegesmund, S. & Kern, H. 1990. Velocity anisotropy and shear wave splitting in mylonites from the Insubric Line (Ivrea-Zone, Italy). *Earth Planet. Sci. Lett.* **99**, 29–47.

Siegesmund, S., Kern, H. & Vollbrecht, A. 1991. The effect of oriented microcracks on seismic velocities in an ultramylonite. *Tectonophysics* **189**, 125–136.

Siegesmund, S., Takeshita, T. & Kern, H. 1989. Anisotropy of V_p and V_s in an amphibolite of the deeper crust and its relationship to the mineralogical, microstructural and textural characteristics of the rock. *Tectonophysics* **157**, 25–38.

Takeshita, T. 1987. Texture development and plastic anisotropy in deformed polycrystals: theories, experiments and geological implications. Unpublished Ph.D. thesis, University of Berkeley, California.

Takeshita, T. & Wenk, H.-R. 1988. Plastic anisotropy and geometrical hardening in quartzites. *Tectonophysics* **149**, 345–361.

Wagner, F., Wenk, H.-R., Esling, C. E. & Bunge, H. J. 1981. Importance of odd coefficients in texture calculations for trigonal triclinic symmetries. *Phys. Status. Solidi.* **A67**, 269–285.

Wurm, F. 1973. Wechselbeziehung kaledonischer Deformationspläne nordöstlich Stavanger (Südwest-Norwegen). *Geol. Rdsch.* **62**, 106–115.